iScience

CellPress
OPEN ACCESS

Article

A helicase-independent role of DHX15 promotes MYC stability and acute leukemia cell survival

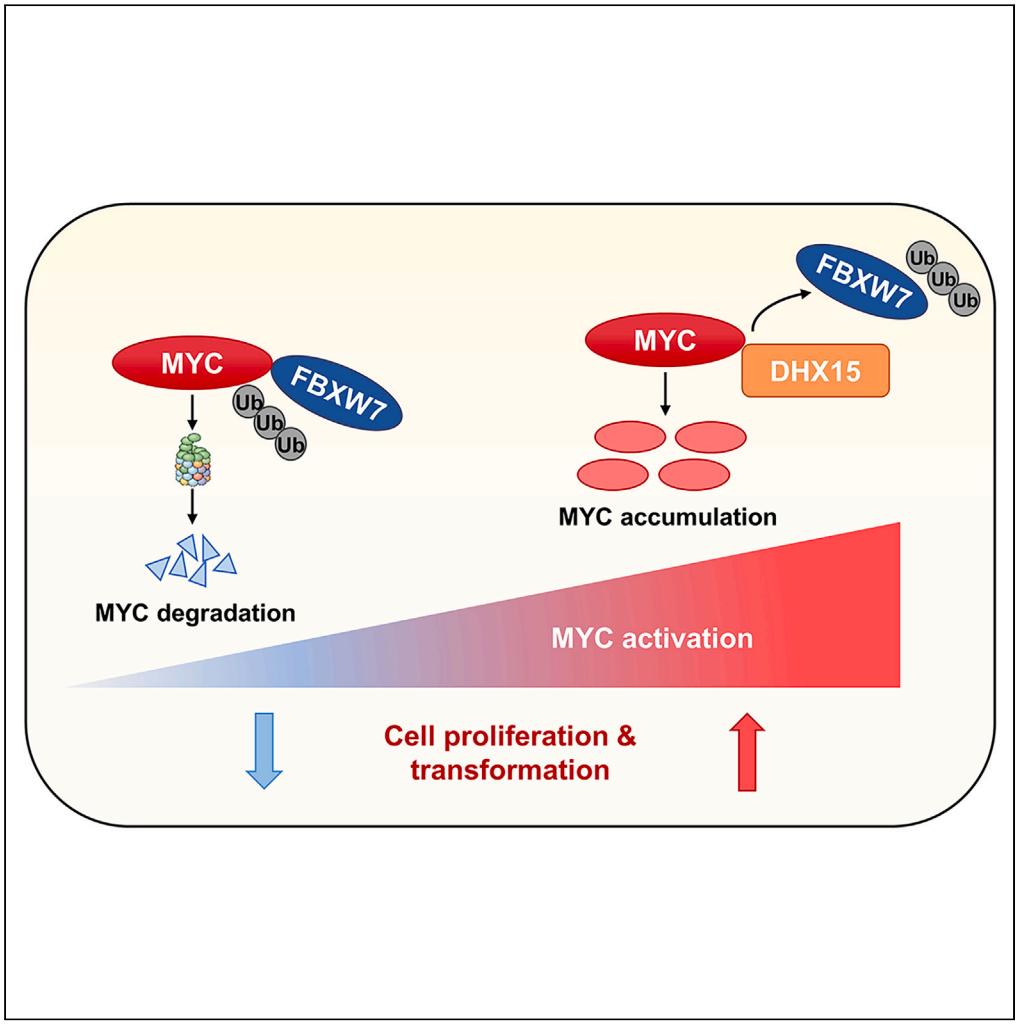

Qilong Li, Hao Guo, Jin Xu, ..., Guoliang Qing, Pieter Van Vlierberghe, Hudan Liu

hudanliu@whu.edu.cn

Highlights

RNA helicase DHX15 directly interacts with and stabilizes MYC oncoprotein

The RNA helicase activity of DHX15 is dispensable for MYC stabilization

DHX15 counteracts FBXW7-mediated ubiquitination and degradation of MYC

The DHX15-MYC axis is required for acute leukemia cell survival

Li et al., iScience 27, 108571
January 19, 2024
https://doi.org/10.1016/j.isci.2023.108571

iScience

CellPress
OPEN ACCESS

Article

A helicase-independent role of DHX15 promotes MYC stability and acute leukemia cell survival

Qilong Li,[1,2,5] Hao Guo,[3,5] Jin Xu,[1,2] Xinlu Li,[1,2] Donghai Wang,[1,2] Ying Guo,[1,2] Guoliang Qing,[1,2] Pieter Van Vlierberghe,[4] and Hudan Liu[1,2,6,*]

SUMMARY

DHX15 has been implicated in RNA splicing and ribosome biogenesis, primarily functioning as an RNA helicase. To systematically assess the cellular role of DHX15, we conducted proteomic analysis to investigate the landscape of DHX15 interactome, and identified MYC as a binding partner. DHX15 co-localizes with MYC in cells and directly interacts with MYC *in vitro*. Importantly, DHX15 contributes to MYC protein stability at the post-translational level and independent of its RNA binding capacity. Mechanistic investigation reveals that DHX15 interferes the interaction between MYC and FBXW7, thereby preventing MYC polyubiquitylation and proteasomal degradation. Consequently, the abrogation of DHX15 drastically inhibits MYC-mediated transcriptional output. While *DHX15* depletion blocks T cell development and leukemia cell survival as we recently reported, overexpression of MYC significantly rescues the phenotypic defects. These findings shed light on the essential role of DHX15 in mammalian cells and suggest that maintaining sufficient MYC expression is a significant contributor to DHX15-mediated cellular functions.

INTRODUCTION

Eukaryotic cells can fine-tune gene expression through a variety of mechanisms, in which many co- and post-transcriptional processes are coordinated by RNA-binding proteins (RBPs).[1,2] RBPs generally form ribonucleoprotein complexes through dynamic interactions with other proteins as well as RNAs, and regulate almost all RNA-processing events, dictating the fate and function of each transcript in the cell and ensuring cellular homeostasis.[1] Increasing evidence suggests that despite the canonical functions at the post-transcriptional regulatory layer, RBPs are implicated in diverse important cellular functions such as the regulation of RNA transcription[2] or being an iron chaperone,[3] shedding light on the previously unrecognized repertoire of RBP functions in the cell.

RNA helicases are a large family of proteins that employ their nucleotide triphosphate (NTP)-dependent activities to remodel RNA structures and RNP complexes in many different cellular processes.[4–7] Most RNA helicases are DEAD or DEAH-box proteins that were initially characterized as RNA duplex unwinders.[5] Over the years, functional studies and biochemical approaches have identified RNA helicases acting in many different aspects of gene expression.[7] DHX15, also termed Prp43 in yeast, is a prominent and extensively characterized multifunctional DEAD/H-box RNA helicase.[8] Accumulating evidence supports that DHX15 plays a crucial role in pre-mRNA splicing by catalyzing the disassembly and recycling of the intron lariat spliceosome (ILS), which marks the end of a splicing cycle.[9–11] In addition, emerging findings suggest that DHX15 may have an expanded role in disassembly of A-complex spliceosomes[12] and in SUGP1-mediated RNA missplicing by mutant SF3B1.[13] Moreover, DHX15 has been shown to release snoRNAs from progenitors of the large ribosomal subunit, thereby involved in ribosome biogenesis and protein synthesis.[14] Prior studies suggest that human DHX15 acts as a viral RNA sensor in antiviral immunity response through the MAVS-mediated signaling pathway[15] and the NLRP6-interferon pathway.[16] All of these cellular functions are based on the RNA-binding property of DHX15, and its catalytic activity is strongly enhanced by the large and diverse class of G-patch activators.[17,18]

The MYC oncoprotein regulates the expression of many genes involved in cell growth, proliferation and metabolic pathway.[19,20] Given the strong growth-promoting activity, MYC abundance is tightly controlled at multiple steps in normal cells, dysregulation of which is often associated with aberrant MYC expression and neoplastic transformation.[21,22] One of the most prominent mechanisms to ensure the proper regulation of MYC involves degradation by the ubiquitin-proteasome system (UPS).[23] MYC protein stability and degradation are regulated by a series of phosphorylation events occurring at the conserved serine 62 and 67 that stabilizes MYC,[24,25] and at the threonine 58 that primes MYC

[1]Department of Hematology, Zhongnan Hospital of Wuhan University, Wuhan University, Wuhan, Hubei 430071, China
[2]Frontier Science Center for Immunology and Metabolism, Medical Research Institute, Wuhan University, Wuhan, Hubei 430071, China
[3]Department of Hematology, The Affiliated Cancer Hospital of Zhengzhou University, Henan Cancer Hospital, Zhengzhou, Henan 450008, China
[4]Department of Biomolecular Medicine, Ghent University, 9000 Ghent, Belgium
[5]These authors contributed equally
[6]Lead contact
*Correspondence: hudanliu@whu.edu.cn
https://doi.org/10.1016/j.isci.2023.108571

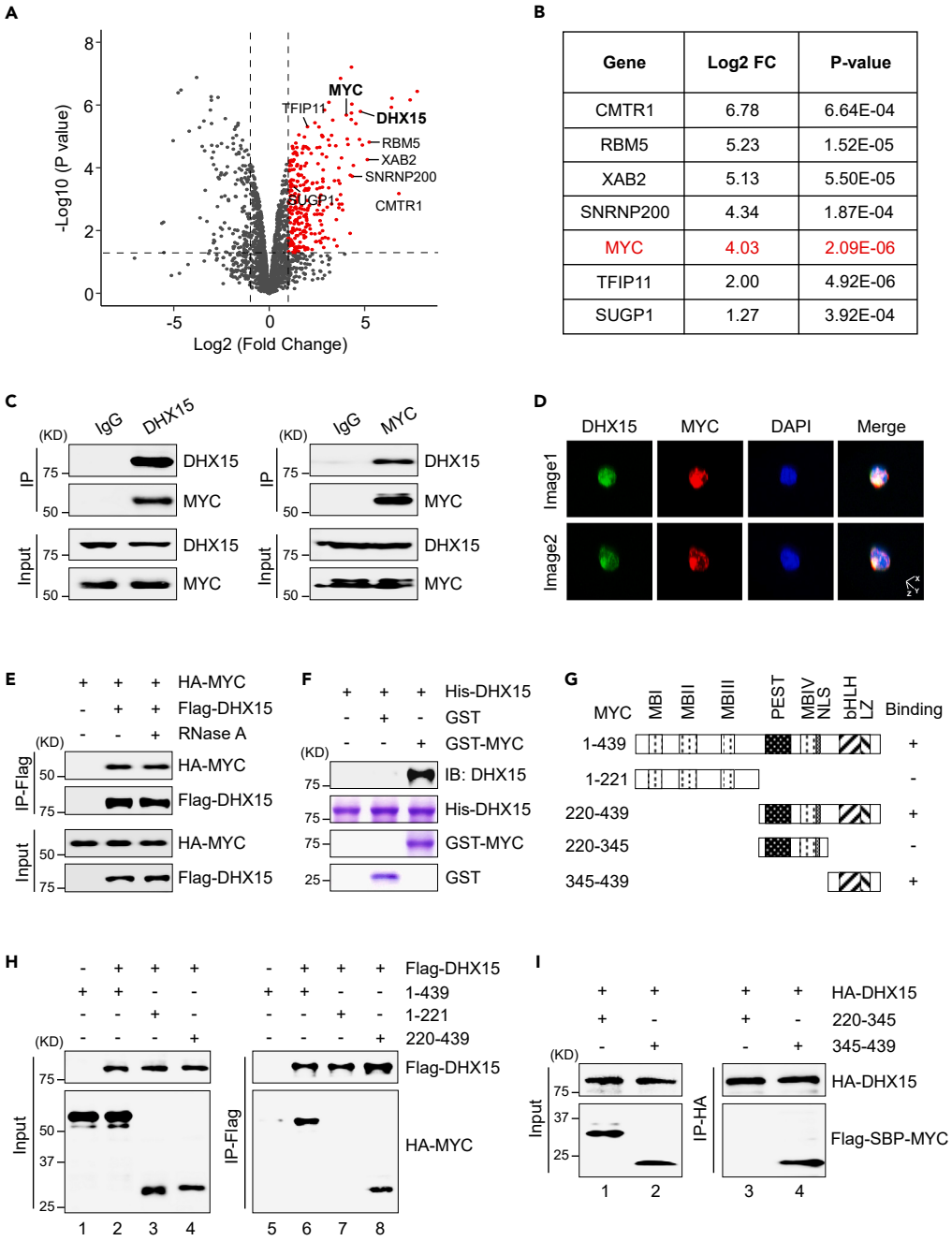

Gene	Log2 FC	P-value
CMTR1	6.78	6.64E-04
RBM5	5.23	1.52E-05
XAB2	5.13	5.50E-05
SNRNP200	4.34	1.87E-04
MYC	4.03	2.09E-06
TFIP11	2.00	4.92E-06
SUGP1	1.27	3.92E-04

Figure 1. DHX15 directly interacts with MYC

(A) Volcano plots showing interacting proteins of DHX15. Associated proteins were immunoprecipitated from human T-ALL CUTLL1 cells using specific DHX15 antibody. Proteins significantly enriched from three independent experiments with a fold change (FC) > 2 and p value <0.05 against the IgG group are displayed as red dots.

(B) MYC and other reported DHX15 binding partners. Fold change and p value of indicated proteins against the IgG group are shown.

(C) CUTLL1 cell lysates were subjected to reciprocal co-IP and immunoblot to detect endogenous DHX15 and MYC interaction. IP: immunoprecipitation.

(D) Immunofluorescence showing the subcellular localization of DHX15 (green) and MYC (red) in CUTTL1 cells. Nuclei were visualized by DAPI staining (blue). These three-dimension (3D) images were captured by the Nikon Eclipse microscope. Scale bar, X/Y: 15.14 μm, Z: 13.71μm.

(E) Lysates of 293T cells co-expressing Flag-tagged DHX15 and HA-tagged MYC were treated with RNase (10 μg/mL) and subjected to co-IP for detecting protein interaction.

(F) GST pull-down to detect direct DHX15 and MYC interaction. Recombinant His-tagged DHX15 was incubated with GST-tagged MYC *in vitro* before pull-down assay with GST beads, and interaction was analyzed by immunoblot. GST: glutathione-S-transferase.

Figure 1. *Continued*

(G) Schematic presentation of various human MYC truncations used in DHX15-binding assays.

(H) Lysates from 293T cells overexpressing Flag-tagged DHX15 and HA-tagged MYC truncations (amino acids 1–221 and 220–439) were subjected to co-IP and immunoblot.

(I) Co-IP of HA-DHX15 and Flag-SBP-fused MYC C-terminal truncations from lysates of 293T cells overexpressing respective tagged proteins. SBP: streptavidin-binding peptide.

ubiquitylation and degradation.[26] The best-studied E3 ubiquitin ligase for MYC is FBXW7, the F box substrate-specificity component of the SCF-type (Skp-Cullin-Fbox) RING-FINGER domain ubiquitin ligase complex,[27,28] loss function of which is frequently found in human cancers.[29]

In a previous study, we conducted a genome-wide RNA splicing analysis in DHX15-deficient T-lymphoblastic leukemia cells, and discovered that loss of *DHX15* resulted in altered RNA splicing of glutamine transporters *SLC7A6* and *SLC38A5*, leading to the suppression of mTORC1 signaling and subsequent leukemia cell death.[30] To further investigate the cellular role of DHX15 in human cells, we performed a proteomic analysis to identify DHX15 interaction partners. Our findings revealed that DHX15 interacts with MYC oncoprotein, along with other known DHX15 binding partners. DHX15 binds to MYC and enhances its protein stability, thereby amplifying the MYC transcriptional output. These findings highlight the activation of the DHX15-MYC axis as a mechanism of action for leukemia cell survival, and also shed light on unconventional roles of RBP in sustaining oncoprotein stability.

RESULTS

DHX15 interatomic analysis identifies MYC as a *bona fide* binding partner

DHX15 has gained increasing attention as a central multitasking RNA helicase[8]; however, a comprehensive review of its interactome remains largely unresolved. We thus exploited specific DHX15 antibody and precipitated endogenous DHX15 and its binding partners from human T cell acute lymphoblastic leukemia (T-ALL) CUTLL1 cells. As shown in Figure 1A, mass spectrometry analysis of the precipitants revealed some well-characterized DHX15 interaction proteins, such as TFIP11, XAB2 and SNRNP200 in the intron-lariat spliceosome complex,[10] CMTR1 involved in mRNA cap-proximal 2′-*O*-methylation,[31,32] RBM5 related to splice site selection[33] and SUGP1 implicated in RNA missplicing mediated by mutant SF3B1.[13] Intriguingly, we found that oncoprotein MYC was ranked among the top candidates in the list of partner proteins (Figure 1B). This observation is reminiscent of our previous interactomic analysis of MYC, which also identified DHX15 as an associated factor.[25] We next performed reciprocal immunoprecipitation using human T-ALL CUTLL1 lysates and confirmed the specific interaction between endogenous DHX15 and MYC in T-ALL cells (Figure 1C). Consistently, three-dimensional immunofluorescence analysis manifested the co-localization of DHX15 and MYC in CUTLL1 cells, supporting physical association between these two proteins in living cells (Figure 1D). We next expressed Flag-tagged DHX15 and HA-tagged MYC in 293T cells for immunoprecipitation, with or without treatment with RNase A, to investigate whether the interaction is RNA-dependent. As depicted in Figure 1E, the physical interaction between DHX15 and MYC remained unchanged even after RNA digestion, suggesting that the interaction is independent of RNA. To further support our findings, we purified recombinant His-DHX15 and GST-MYC from *E. coli* extract and performed a GST pull-down assay. The results showed that GST-MYC specifically precipitated His-DHX15, indicating a direct protein-protein interaction between DHX15 and MYC (Figure 1F).

To determine the precise region(s) in MYC for this interaction, we simultaneously expressed full-length Flag-tagged DHX15 and HA-tagged fragments of MYC in 293T cells (Figure 1G). The N-terminal region of MYC (amino acids 1–221) containing the first three MYC box (MB) domains failed to interact with DHX15, whereas the C-terminal region (amino acids 220–439) showed robust binding signals (Figure 1H, Lanes 7–8). To further define the interacting module, we co-expressed the HA-tagged DHX15 in combination with truncated fragments of the MYC C-terminal region (amino acids 220–345 and 345–439) fused with Flag-tagged Streptavidin-Binding Peptide (SBP). Co-immunoprecipitation revealed that the MYC 345–439 fragment displayed robust binding to DHX15 (Figure 1I, Lanes 3–4), suggesting a minimal binding motif for MYC interaction with DHX15. DHX15 consists of multiple domains and exhibits both ATPase and helicase activities (Figure S1A). We further identified the Ratchet domain (amino acids 566–676) as the key region responsible for mediating the interaction with MYC (Figure S1). These findings thus provide compelling evidence supporting MYC as a *bona fide* interacting partner of DHX15.

DHX15 loss inhibits MYC protein expression and transcriptional activity

To assess the mutual regulation between DHX15 and MYC, we respectively knocked down *DHX15* or *MYC* in CUTLL1 and KOPTK1 cells by short hairpin RNAs (shRNAs). While *MYC* deficiency had minimal impact on DHX15 expression, depletion of *DHX15* resulted in a significant reduction in MYC protein levels, despite minimal change in *MYC* mRNA expression (Figures 2A and S2A). Downregulation of MYC protein was also observed in murine T-lymphoblasts derived from NOTCH1-induced T-ALL model in the absence of *Dhx15* expression,[30] whereas *Myc* mRNA was barely changed (Figure 2B). This regulatory DHX15-MYC axis can be generalized to other tumor contexts, as the depletion of *DHX15* consistently resulted in reduced MYC protein expression in human acute myeloid leukemia (AML) cells such as Kasumi-1, HL-60 and OCI-AML3, as well as colon cancer RKO and lung cancer H1299 cells (Figures S2B and S2C).

Consistent with these findings, RNA sequencing (RNA-seq) analysis conducted in *DHX15*-depleted CUTLL1 cells and NOTCH1-induced murine T-lymphoblasts revealed significant enrichment of MYC target gene sets (Figures 2C and 2D). We recently reported a single-cell transcriptomic profiling of murine thymocytes and identified a highly proliferating cluster of $CD4^{-}CD8^{-}$ (DN)-to-$CD4^{+}CD8^{+}$ (DP) transitional cells (DN/DPtrans) which exhibit most differentially expressed genes with or without *Dhx15* expression.[30] Comparison of the differential genes

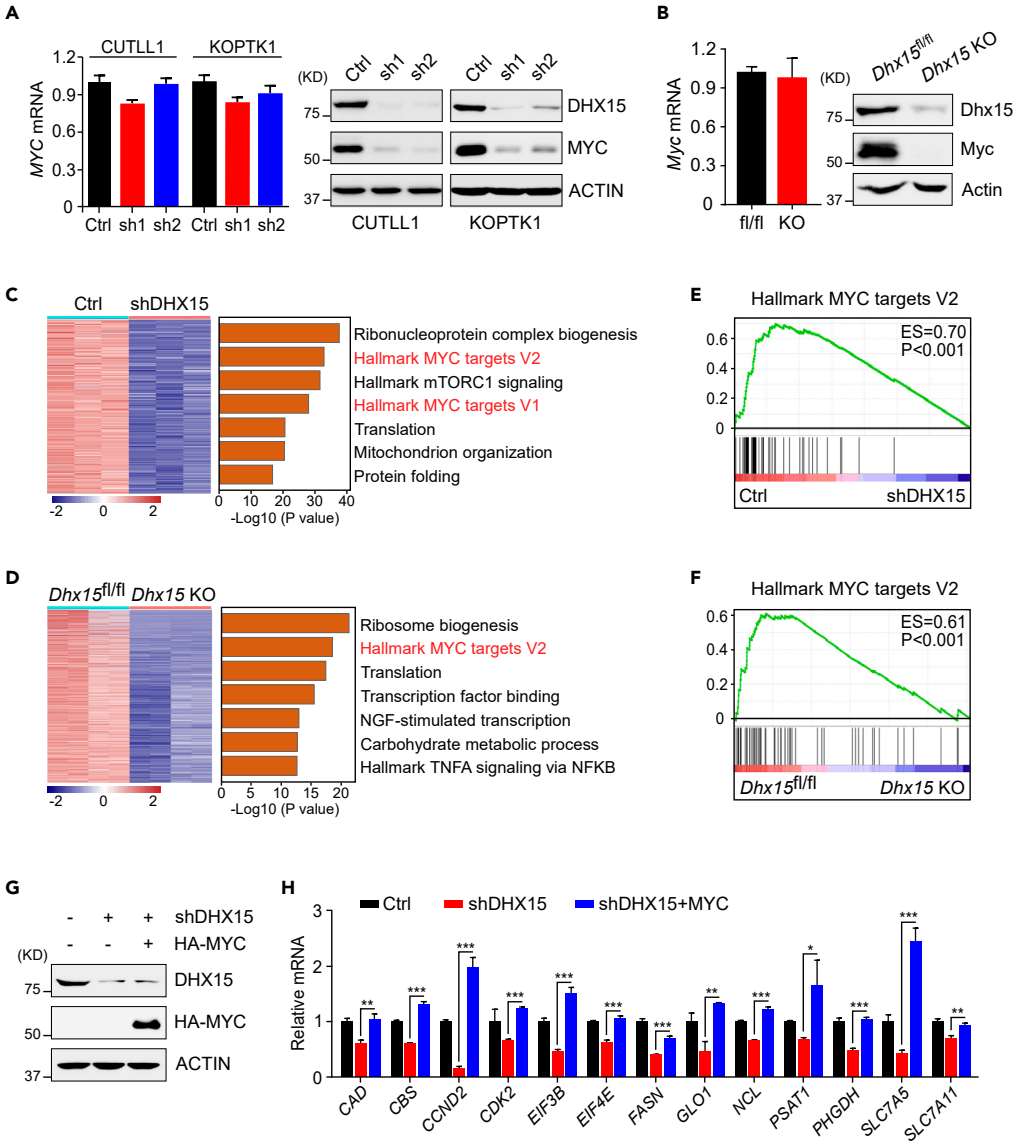

Figure 2. *DHX15* depletion attenuates the MYC protein accumulation and transcriptional activity

(A) CUTLL1 and KOPTK1 cells were transduced with lentiviruses expressing shRNA targeting control (Ctrl) or *DHX15* (sh1: targeting 3′UTR and sh2: targeting coding region). *MYC* mRNA and protein were analyzed by qPCR (left) and immunoblot (right).

(B) NOTCH1-induced T-ALL model was established via retroviral transduction and bone marrow transplantation. *MYC* mRNA and protein were analyzed by qPCR and immunoblot in GFP$^+$ spleen-infiltrating cells from T-ALL mice with *Dhx15* $^{fl/fl}$ and *Dhx15* KO (*Lck*-cre *Dhx15* $^{fl/fl}$) as bone marrow donors.[30]

(C and D) Heatmap showing significantly downregulated genes (false discovery rate (FDR) < 0.01, fold change<−1.5) in CUTLL1 cells (C) and murine blasts (D) upon *DHX15* withdrawal as shown in (A and B). Gene enrichment analysis was performed by Metascape (www.metascape.org) and the enriched terms were illustrated and aligned by p values.

(E and F) Gene Set Enrichment Analysis (GSEA) of MYC-regulated gene signatures in CUTLL1 cells (E) and murine T-lymphoblasts (F) with or without *DHX15* depletion as shown in (A and B).

(G) KOPTK1 cells were transduced with lentiviruses expressing *DHX15* shRNA (sh1 in Figure 2A) or in combination with the ectopic expression of *MYC* coding region. DHX15 and MYC proteins were analyzed by immunoblot.

(H) qPCR validation of representative MYC target genes in *DHX15*-depleted KOPTK1 cells with exogenous MYC expression. Data shown represent the means (±SD) of three biological replicates, *p < 0.05, **p < 0.01, ***p < 0.001; significance was determined by one-way ANOVA test followed by Tukey's correction.

revealed that *Dhx15* knockout significantly inhibited the expression of MYC signature genes as well (Figure S2D), suggesting a shared regulatory mechanism in normal and transformed T cells. Gene set enrichment analysis (GSEA) further supported our findings, revealing that *DHX15* depletion resulted in significant decline in the MYC-induced gene expression profile in human and mouse T-ALL cells as well as the DN/DPtrans cluster cells (Figures 2E, 2F, and S2E). Of note, 192 genes (74.4%) from the datasets of Hallmark MYC targets V1 and V2

(n = 258) were downregulated in *DHX15* deficient CUTLL1 cells (Figure S2F).[34] Subsequently, we conducted qPCR to assess the expression of a panel of well-characterized MYC target genes and confirmed their downregulation upon *DHX15* withdrawal (Figure S2G). To confirm the pivotal role of MYC as a significant downstream target of DHX15, we performed the transcriptome analysis in *DHX15*-depleted KOPTK1 cells while MYC was restored. Indeed, majority of down-regulated genes were efficiently rescued by MYC overexpression (Figure S2H). As a further support, multiple canonical MYC target genes were robustly reactivated when MYC was restored in *DHX15*-depleted KOPTK1 cells (Figures 2G and 2H).

To exclude the possibility that loss of *DHX15* impacts *MYC* mRNA splicing, we checked the read counts for all *MYC* exons and introns in our RNA-seq data. Genome browser tracks showed that *DHX15* depletion in CUTLL1 cells did not cause noticeable changes in the exon peaks of *MYC* mRNA (Figure S3A). Of note, both *MYC* mature and pre-mRNA were barely changed (Figure S3B), as did two distinct transcript variants of *MYC* (Figure S3C). These findings underscore the activation of MYC transcriptional program as a key molecular event in mediating the function of DHX15, and suggest that the DHX15 modulation of MYC transcriptional program is most likely to involve mechanisms other than altering splicing of *MYC* transcripts.

DHX15 depletion induces MYC ubiquitylation-proteasome degradation

DHX15 could potentially affect MYC protein levels through the regulation of MYC protein synthesis or degradation. The implication of DHX15 in ribosome biogenesis, as suggested by previous studies,[14,35] raises the possibility that DHX15 may affect MYC protein synthesis. However, it was observed that *DHX15* deficiency did not alter the distribution of *MYC* mRNA in polysomal fractions, which suggests that the loss of DHX15 may not directly impair MYC protein synthesis (Figure S3D). Rapid protein degradation by the ubiquitin-proteasome system is an essential mechanism responsible for tight control of MYC protein abundance.[36] Time-course experiments unveiled a significant reduction in the half-life of endogenous MYC in both T-ALL KOPTK1 and AML HL-60 cells upon *DHX15* depletion. Moreover, the expedited degradation of MYC protein was notably ameliorated upon the reconstitution of DHX15 wild-type (WT) or the helicase inactive mutant (K166A)[15] into *DHX15*-depleted KOPTK1 and HL-60 cells, resulting in substantial MYC accumulation (Figures 3A–3C). These results indicate that DHX15 plays a general role in maintaining MYC stability independent of its helicase activity. Consistently, overexpression of DHX15 WT or K166A also effectively rescued the downregulation of MYC target genes (Figure S4A). As the reduction of MYC protein was efficiently rescued by the proteasome inhibitor MG132 (Figure 3D), we reasoned that MYC was subjected to rapid proteasomal degradation upon *DHX15* withdrawal. Further supporting this observation, the ubiquitylation assay revealed robust polyubiquitylation signals on endogenous MYC proteins upon *DHX15* depletion (Figures 3E and 3F). This finding suggests that DHX15 plays a crucial role in preventing the polyubiquitylation of MYC before proteasomal degradation, highlighting its significance in regulating MYC protein stability.

DHX15 counteracts FBXW7 to promote MYC stability

In line with the findings in leukemia cells, the enforced expression of either exogenous DHX15 WT or K166A in 293T cells led to markedly prolonged half-life of MYC protein (Figures 4A and 4B). Recent studies have indicated that the DEAD-box RNA helicases act as global regulators of phase-separated organelles[37] and DHX15 has been implicated in anti-viral immunity through phase separation.[38] The N-terminus of DHX15 (amino acids 1–109) features an intrinsically disordered region (IDR), essential for initiating phase separation, as assessed by MetaDisorder analysis (Figure S4B). Both recombinant full-length DHX15 and the isolated IDR region successfully formed droplets in the presence of the crowding agent PEG8000 *in vitro* (Figure S4C). Furthermore, fluorescence microscopy images consistently demonstrated that DHX15 IDR, as opposed to the helicase domain (amino acids 110–795, non-IDR), induced the formation of phase-separated droplets within living cells (Figure S4D). However, our findings revealed that the DHX15-mediated stabilization of MYC was not dependent on liquid-liquid phase separation (LLPS), as DHX15 truncations lacking LLPS competency (amino acids 110–795) were still able to stabilize MYC, while DHX15 IDR failed to do so (Figures 4A and 4B). Subsequently, we checked the interaction between these DHX15 mutants/truncates with MYC by immunoprecipitations. As expected, DHX15 K166A and DHX15 non-IDR that significantly extend the half-life of MYC exhibited the capacity of MYC binding, whereas DHX15 IDR did not manifest this binding capability (Figure S4E).

We next assess the interplay between DHX15 and FBXW7, the major MYC E3 ligase, in the coordinated regulation of MYC stability. Depletion of *FBXW7* in CUTLL1 cells expressing *DHX15* shRNA resulted in the de-repression of MYC abundance (Figure 4C), suggesting that MYC degradation induced by *DHX15* loss is dependent on FBXW7. Conversely, enforced DHX15 expression rescued MYC abundance that was downregulated by the co-expression of FBXW7 (Figure 4D), and moreover, inhibited the polyubiquitylation reaction mediated by FBXW7 (Figure 4E). It is noteworthy that increasing doses of DHX15 expression abolished MYC and FBXW7 interaction (Figure 4F), suggesting that DHX15 competes with FBXW7 for binding to MYC. Collectively, our findings reveal a previously unrecognized mechanism by which DHX15 promotes MYC protein stability through physical protein interaction, thereby blocking FBXW7-mediated MYC polyubiquitylation and subsequent degradation.

The DHX15-MYC axis is required for T cell development and leukemia cell survival

To elucidate the biological significance of the DHX15-MYC axis, we ectopically enforced MYC expression in *DHX15*-deficient T-ALL KOPTK1 cells and AML HL-60 cells. Consistent with earlier findings,[30] DHX15 ablation significantly inhibited cell growth and triggered considerable cell death. Remarkably, we observed a significant rescue of cell viability and growth defects resulting from *DHX15* loss, indicating that MYC overexpression can compensate for the adverse effects of *DHX15* deficiency in these cells (Figures 5A–5C and S5). As MYC is equally important during normal T cell development, we also explored the regulatory mechanism in this physiological context.

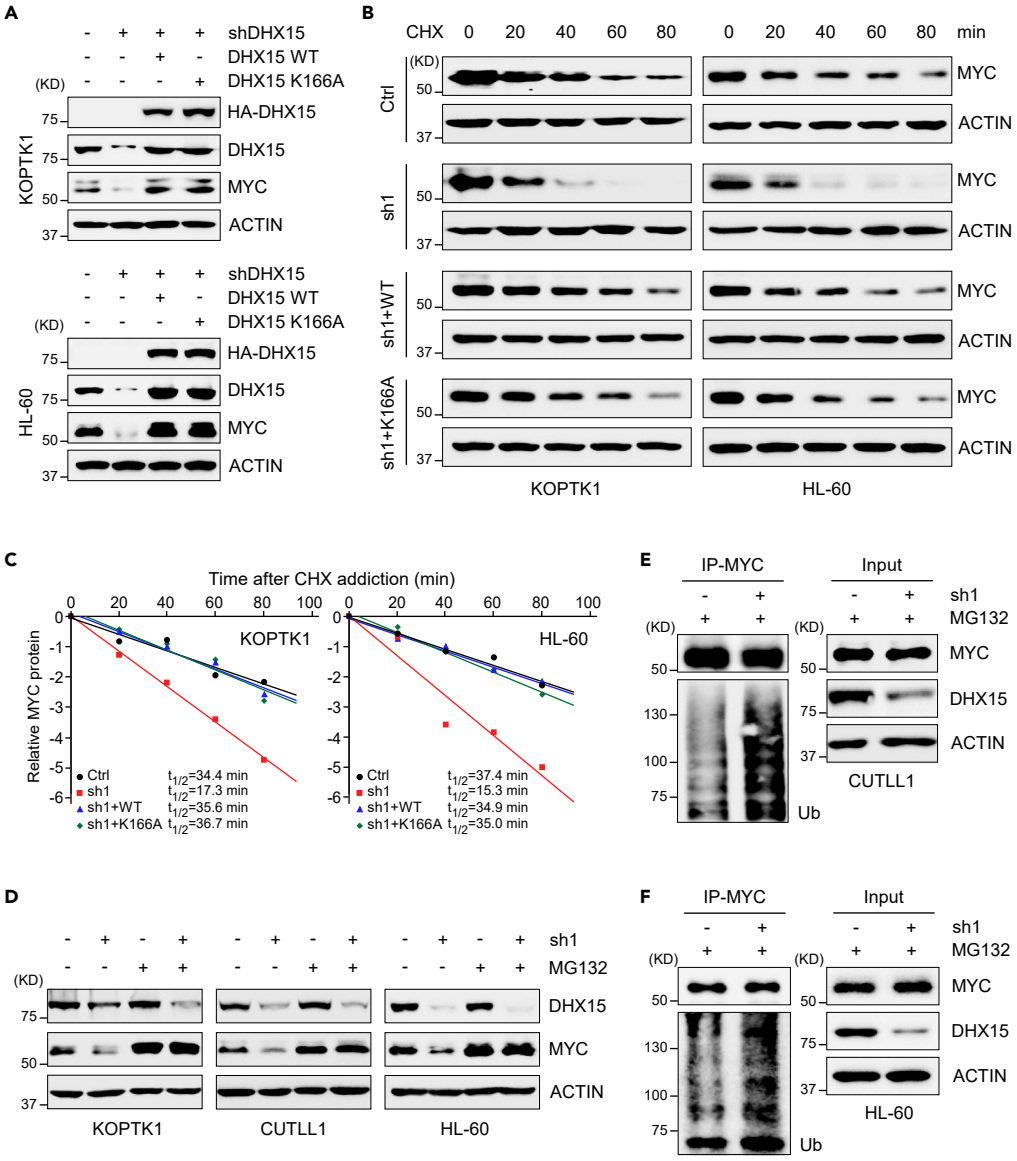

Figure 3. DHX15 inhibition promotes MYC ubiquitylation-proteasomal degradation

(A) KOPTK1 and HL-60 cells were transduced with lentiviruses expressing *DHX15* shRNA (sh1 in Figure 2A) or in combination with the ectopic expression of DHX15 wild-type (WT) or mutant (K166A). DHX15 and MYC proteins were analyzed by immunoblot.

(B and C) Time-course analysis of MYC protein in *DHX15*-depleted KOPTK1 and HL-60 cells with or without DHX15 WT or DHX15 K166A expression (B). MYC proteins were quantified and plotted as shown in (C).

(D) *DHX15*-depleted KOPTK1, CUTLL1 and HL-60 cells were treated with MG132 (10 μM) for 6 hr before harvest. MYC protein was analyzed by immunoblot.

(E and F) Analysis of endogenous MYC polyubiquitylation upon *DHX15* depletion. Denaturing protein IP with anti-MYC antibody and immunoblots were performed in CUTLL1 (E) and HL-60 (F) cells with or without *DHX15* depletion.

Immunoblots confirmed the concomitant decrease of Myc expression with *Dhx15* knockout in multiple fractions of T cell progenitors (DN2-4) (Figure S6A). Based on the resemblance of impaired T cell proliferation observed in T cell lineage-specific ablation of *Dhx15* and *Myc*,[30,39] we postulated that the decreased T cell proliferation induced by *Dhx15* knockout is likely attributed to the downregulation of Myc expression. To address this hypothesis, we enforced Myc expression in *Dhx15* $^{fl/fl}$ or *Dhx15* KO (*Lck*-cre *Dhx15* $^{fl/fl}$) bone marrow hematopoietic progenitors and transplanted them into immunodeficient NOD.Cg-Prkdc^{scid} Il2rg^{tm1Vst}/Vst (NPG) mice (Figures 5D and S6B). As shown in Figures 5E and 5F, bone marrow hematopoietic progenitors without *Dhx15* expression failed to complete T cell reconstitution, while the ectopic expression of *Myc* restored the capacity to yield mature T cells. As enforced MYC expression only partially rescued the defects in normal or transformed T cell proliferation and survival, DHX15 likely exerts its biological functions through multiple mechanisms. Other pathways such as mTORC1, as we previously reported,[30] may also contribute to the overall biological function of

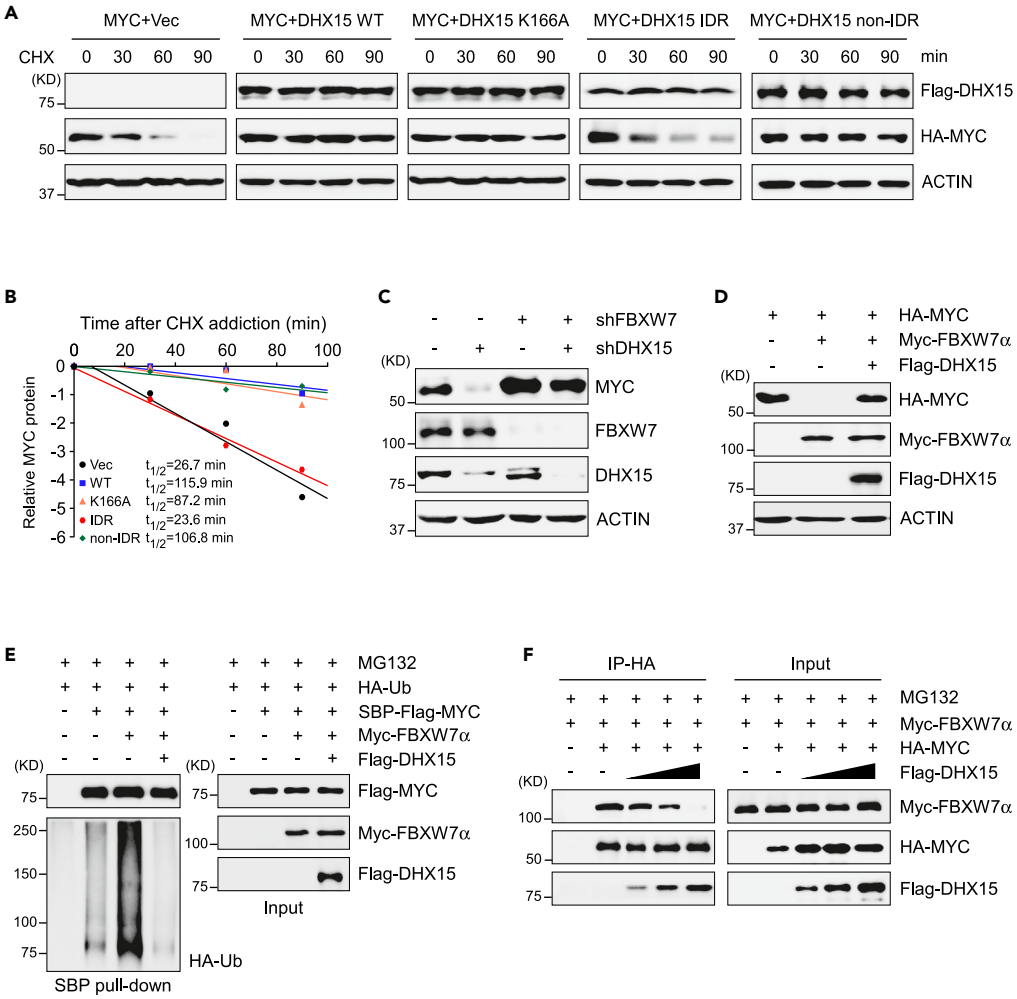

Figure 4. DHX15 enhances MYC protein stability via antagonizing FBXW7

(A and B) Time-course analysis of HA-tagged MYC protein levels in 293T cells co-expressing Flag-tagged DHX15 wild-type (WT), mutant (K166A) or truncations (IDR: amino acids 1–109 and non-IDR: amino acids 110–795) as indicated. Ectopic MYC proteins were quantified and plotted as shown in (B). IDR: intrinsically disordered region.

(C) *FBXW7* was depleted by shRNA in CUTLL1 cells with or without *DHX15* depletion. MYC protein was analyzed by immunoblot.

(D) Immunoblot analysis in 293T cells co-expressing HA-tagged MYC, Myc-tagged FBXW7α and Flag-tagged DHX15 as indicated.

(E) Analysis of MYC polyubiquitylation. Denaturing proteins from 293T cells expressing indicated constructs were pulled down with streptavidin beads and subjected to immunoblot analysis. MG132 (10 μM) was added in 293T cells for 6 hr before harvest. SBP: streptavidin-binding peptide.

(F) Protein interaction between FBXW7α and MYC in the presence of DHX15. Lysates of 293T cells co-expressing Myc-tagged FBXW7α, HA-tagged MYC and increasing doses of Flag-tagged DHX15 were subjected to co-IP for detecting protein interaction. MG132 (10 μM) was added in 293T cells for 6 hr before harvest.

DHX15. Nevertheless, our findings underscore the essential mechanism of DHX15 in regulating MYC stability, which plays a crucial role in both T cell development and leukemia.

DISCUSSION

RNA-binding proteins (RBPs) are generally known to interact with RNA molecules through their RNA-binding domains, which allow them to regulate various aspects of RNA metabolism, including RNA splicing, stability, transport and translation. Accordingly, RBPs are critical for many cellular processes and dysregulation of RBPs has been implicated in a wide range of human diseases, including cancer.[40,41] Interestingly, emerging findings suggest that RBPs may exert cellular functions that are independent of their RNA-binding properties.[2] We previously show that the DEAH-box family of RNA helicase DHX15 plays a pivotal role in acute T cell leukemia via modulating RNA splicing of crucial genes in mTORC1 pathway.[30] In this study, we report an unprecedented RNA-binding independent function of DHX15 that acts as a binding partner of MYC oncoprotein, contributing to MYC stability and transcriptional program. The DHX15-MYC regulatory axis represents an

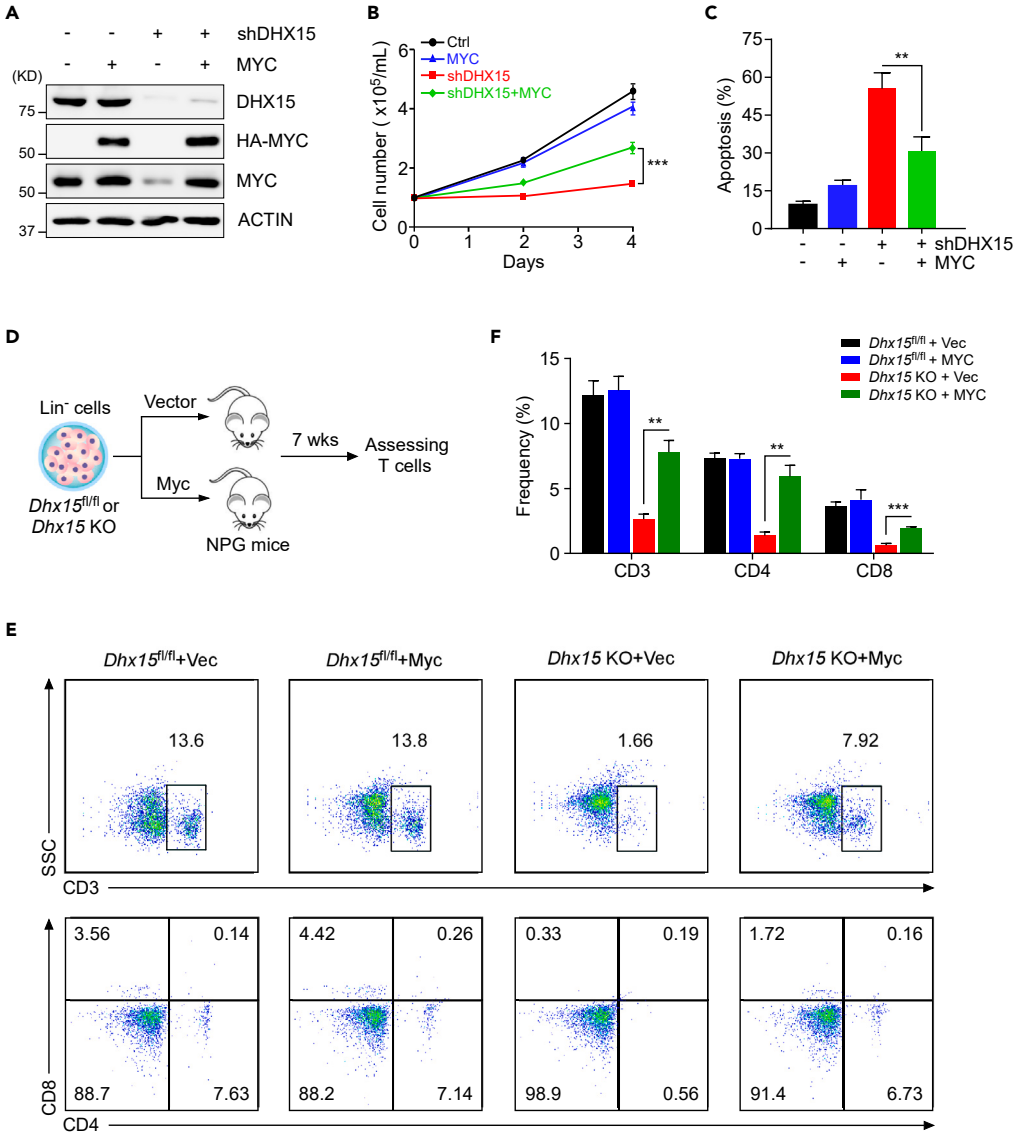

Figure 5. The DHX15-MYC axis is required for leukemia cell survival and normal T cell development

(A–C) KOPTK1 cells were transduced with lentiviruses expressing *DHX15* shRNA (sh1 in Figure 2A) and/or *MYC* coding region. DHX15 and MYC proteins were analyzed by immunoblot (A). Cells were counted at the indicated time points and cell growth was plotted as shown in (B). Apoptotic cell death was analyzed by Annexin V-PI staining (C).

(D) Graphic illustration of *in vivo* T cell reconstitution experiment. Lin^- BM cells from *Dhx15* $^{fl/fl}$ or *Dhx15* KO (*Lck*-cre *Dhx15* $^{fl/fl}$) mice were transduced with MigR1 vector (Vec) or MigR1-Myc retroviruses, and then transplanted into irradiated immunodeficient NPG mice, followed by the assessment of T cell generation.

(E) Representative flow cytometry analysis of $CD3^+$ T cells (upper) and $CD4^+$ and $CD8^+$ T cells (bottom) in the peripheral blood (PB) of NPG mice 7 weeks post-transplant.

(F) Quantification of reconstituted $CD3^+$, $CD4^+$ and $CD8^+$ T cell populations in each group (n = 4). Data are mean ± SD, $^{**}p < 0.01$, $^{***}p < 0.001$; significance was determined by one-way (C and F) or two-way (B) ANOVA test followed by Tukey's correction.

important mechanism of action underlying leukemia cell proliferation and survival, highlighting its significance in the context of leukemia pathogenesis.

DHX15 was first identified as a putative RNA helicase with RNA-unwinding activity[42] and its precise role in the last step of splicing was reported in yeast by facilitating the disassembly of spliceosome and release of lariat.[9] DHX15 has recently gained increasing attentions as an extensively characterized multifunctional RNA helicase involved in multiple aspects of RNA metabolism.[8] In support of this notion, we and others have recently reported cellular function of DHX15 in altering RNA splicing in acute leukemia.[30,43,44] Intriguingly, we herein revealed an unexpected and important mechanism of action that DHX15 protects MYC from degradation by the ubiquitylation-proteasome system.

FBXW7 is the primary E3 ligase responsible for MYC proteasomal degradation. Notably, DHX15 and FBXW7 do not share the same minimal binding region within MYC that DHX15 interacts with the "bHLH/LZ" region, whereas FBXW7 binds to the MYC MB I.[27] We therefore reason that DHX15 association with MYC very likely creates a steric hindrance for FBXW7 to bind the substrate, thereby conferring to enhanced MYC protein stability. We particularly ruled out the possibility that DHX15 acts as a potential deubiquitylase in this scenario by an *in vitro* deubiquitylation assay (data not shown). Intriguingly, DHX15 mutations, especially the hot spot *R222G*, were recurrently found in AML with RUNX1-RUNXT1 fusion.[44] Our unpublished data show that DHX15 *R222G* retains the capacity of binding with MYC and enhancing its stability. This mutation therefore may exert pro-leukemogenic function through other mechanisms. Moreover, DEAD/H family proteins can serve as global regulators of phase-separated organelles.[37] However, our data suggest that DHX15-mediated phase separation is not required for MYC protein stability. Recent work unraveled versatile functions of DHX15 in human diseases independent of its ATPase activity or RNA-binding capacity.[45,46] These findings, together with ours, argue a prominent role of DHX15 in protein-protein interaction network beyond canonical RBP functions. Interestingly, a separate study revealed that another RNA helicase DDX5 interacts with MYC, regulating MYC transcriptional activity rather than its stability,[47] highlighting the importance of RNA helicases in regulating MYC through multiple mechanisms.

According to our previous study, *DHX15* knockout in T cell lineage led to severe defects in T cell development characterized by atrophic size and reduced the cellularity of the thymus, resulting in the decrease of peripheral CD4/8 T cells in both spleen and blood.[30] We here show that *DHX15* loss depletes MYC, consequently leading to T cell development defect. Indeed, *Lck*-Cre-mediated *MYC* ablation resembles the phenotype of conditional *Dhx15* knockout in thymocytes.[39,48] Exogenous MYC expression significantly restores the T cell number in the peripheral blood of *Dhx15* knockout mice, demonstrating that MYC is a primary downstream effector of DHX15 that plays a crucial role in T cell development. More importantly, the DHX15-MYC regulatory axis underlying the physiological pre-T cell proliferation can be hijacked during leukemogenesis. As unchecked cell propagation can result in predispose to human T-ALL,[49] controlled the proliferation of progenitor cells is necessary to avoid cellular transformation leading to T-ALL. Thus, inhibiting MYC expression or activity should have an important clinical relevance for T-ALL treatment. Given that no direct MYC inhibitor has been tested in clinical trials, the identification of RBPs engaged in the regulation of MYC-dependent transcriptional program points to an alternative way to be harnessed to aid the development of targeted therapies.

In sum, we provide an example of how a canonical RBP participates in the oncoprotein interaction network and contributes to the development of human cancer. Our findings emphasize the critical role of RBPs in cancer development and provide insights into the complex regulatory mechanisms underlying cancer-associated gene expression changes. RBPs can exhibit diverse cellular functions beyond their RNA-binding activity, and their RNA-binding independent functions are increasingly recognized as important regulatory mechanisms in cellular physiology and pathology. Further research is expected to fully decipher the molecular mechanisms underlying the RNA-binding independent functions of RBPs and their roles in cellular processes.

Limitations of the study

Our study reports an unexpected and pivotal mechanism wherein DHX15 disrupts the interaction between MYC and FBXW7, consequently impeding MYC polyubiquitylation and proteasomal degradation. While we reason that the DHX15 association with MYC likely creates steric hindrance for FBXW7 in substrate binding, the precise mechanism by which DHX15 counteracts FBXW7 remains elusive. In a prior study, we demonstrated DHX15 as a causative factor for typical RNA metabolism abnormalities, impacting leukemia cell survival and T cell progenitor proliferation.[30] To what extent this uncanonical role of DHX15 in the regulation of MYC contributes to T-ALL progression awaits further evaluation. Moreover, numerous proteins contribute to bolstering the MYC protein stability, yet the specific function DHX15 fulfills to stabilize MYC within cellular context remains enigmatic.

STAR★METHODS

Detailed methods are provided in the online version of this paper and include the following:

- KEY RESOURCES TABLE
- RESOURCE AVAILABILITY
  - Lead contact
  - Materials availability
  - Data and code availability
- EXPERIMENTAL MODEL AND STUDY PARTICIPANT DETAILS
  - Cell lines
  - Animals
  - Microbe strains
- METHOD DETAILS
  - Lentiviral and retroviral transduction
  - RNA extraction and quantitative real-time PCR
  - Immunoblotting
  - Co-immunoprecipitation
  - Immunofluorescence
  - Time-course analysis of MYC degradation

- *In vivo* T-cell reconstitution
- RNA sequencing
- Mass spectrometry analysis
- Flow cytometry analysis

- QUANTIFICATION AND STATISTICAL ANALYSIS

SUPPLEMENTAL INFORMATION

Supplemental information can be found online at https://doi.org/10.1016/j.isci.2023.108571.

ACKNOWLEDGMENTS

We thank members of the Liu and Qing Laboratories for helpful suggestions and the Core Facility of Medical Research Institute at Wuhan University for flow sorting. This study was supported by grants from the National Natural Science Foundation of China (82161138024, 82025003 and 82011530151 to HL, 81830084 to GQ, 82301964 to HG), Hubei Provincial Natural Science Fund for Creative Research Groups (2021CFA003 to HL), the Natural Science Foundation of Henan (232300421280 to HG) and the Research Foundation Flanders (G0E6222N to PVV).

AUTHOR CONTRIBUTIONS

HL conceived and designed the study. PVV provides conceptual suggestions and support. HL supervised the study and wrote the article. QL and HG performed most of the experiments. JX and XL helped with animal experiments and plasmid constructions. YG performed mass spectrometry analysis. DW analyzed the RNA-Seq data.

DECLARATION OF INTERESTS

The authors declare no competing interests.

Received: May 17, 2023
Revised: October 13, 2023
Accepted: November 21, 2023
Published: November 23, 2023

REFERENCES

1. Glisovic, T., Bachorik, J.L., Yong, J., and Dreyfuss, G. (2008). RNA-binding proteins and post-transcriptional gene regulation. FEBS Lett. *582*, 1977–1986.
2. Xiao, R., Chen, J.Y., Liang, Z., Luo, D., Chen, G., Lu, Z.J., Chen, Y., Zhou, B., Li, H., Du, X., et al. (2019). Pervasive Chromatin-RNA Binding Protein Interactions Enable RNA-Based Regulation of Transcription. Cell *178*, 107–121.e118.
3. Patel, S.J., Protchenko, O., Shakoury-Elizeh, M., Baratz, E., Jadhav, S., and Philpott, C.C. (2021). The iron chaperone and nucleic acid-binding activities of poly(rC)-binding protein 1 are separable and independently essential. Proceedings of the National Academy of Sciences of the United States of America *118*.
4. Jarmoskaite, I., and Russell, R. (2014). RNA helicase proteins as chaperones and remodelers. Annu. Rev. Biochem. *83*, 697–725.
5. Linder, P., and Jankowsky, E. (2011). From unwinding to clamping - the DEAD box RNA helicase family. Nat. Rev. Mol. Cell Biol. *12*, 505–516.
6. Sloan, K.E., and Bohnsack, M.T. (2018). Unravelling the Mechanisms of RNA Helicase Regulation. Trends Biochem. Sci. *43*, 237–250.
7. Bourgeois, C.F., Mortreux, F., and Auboeuf, D. (2016). The multiple functions of RNA helicases as drivers and regulators of gene expression. Nat. Rev. Mol. Cell Biol. *17*, 426–438.
8. Bohnsack, K.E., Kanwal, N., and Bohnsack, M.T. (2022). Prp43/DHX15 exemplify RNA helicase multifunctionality in the gene expression network. Nucleic acids research *50*, 9012–9022.
9. Arenas, J.E., and Abelson, J.N. (1997). Prp43: An RNA helicase-like factor involved in spliceosome disassembly. Proceedings of the National Academy of Sciences of the United States of America *94*, 11798–11802.
10. Wan, R., Yan, C., Bai, R., Lei, J., and Shi, Y. (2017). Structure of an Intron Lariat Spliceosome from Saccharomyces cerevisiae. Cell *171*, 120–132.
11. Zhang, X., Zhan, X., Yan, C., Zhang, W., Liu, D., Lei, J., and Shi, Y. (2019). Structures of the human spliceosomes before and after release of the ligated exon. Cell Res. *29*, 274–285.
12. Maul-Newby, H.M., Amorello, A.N., Sharma, T., Kim, J.H., Modena, M.S., Prichard, B.E., and Jurica, M.S. (2022). A model for DHX15 mediated disassembly of A-complex spliceosomes. RNA *28*, 583–595.
13. Zhang, J., Huang, J., Xu, K., Xing, P., Huang, Y., Liu, Z., Tong, L., and Manley, J.L. (2022). DHX15 is involved in SUGP1-mediated RNA missplicing by mutant SF3B1 in cancer. Proceedings of the National Academy of Sciences of the United States of America *119*, e2216712119.
14. Bohnsack, M.T., Martin, R., Granneman, S., Ruprecht, M., Schleiff, E., and Tollervey, D. (2009). Prp43 bound at different sites on the pre-rRNA performs distinct functions in ribosome synthesis. Mol. Cell *36*, 583–592.
15. Mosallanejad, K., Sekine, Y., Ishikura-Kinoshita, S., Kumagai, K., Nagano, T., Matsuzawa, A., Takeda, K., Naguro, I., and Ichijo, H. (2014). The DEAH-box RNA helicase DHX15 activates NF-κB and MAPK signaling downstream of MAVS during antiviral responses. Sci. Signal. *7*, ra40.
16. Wang, P., Zhu, S., Yang, L., Cui, S., Pan, W., Jackson, R., Zheng, Y., Rongvaux, A., Sun, Q., Yang, G., et al. (2015). Nlrp6 regulates intestinal antiviral innate immunity. Science (New York, N.Y.) *350*, 826–830.
17. Bohnsack, K.E., Ficner, R., Bohnsack, M.T., and Jonas, S. (2021). Regulation of DEAH-box RNA helicases by G-patch proteins. Biol. Chem. *402*, 561–579.
18. Studer, M.K., Ivanović, L., Weber, M.E., Marti, S., and Jonas, S. (2020). Structural basis for DEAH-helicase activation by G-patch proteins. Proceedings of the National Academy of Sciences of the United States of America *117*, 7159–7170.
19. Dong, Y., Tu, R., Liu, H., and Qing, G. (2020). Regulation of cancer cell metabolism: oncogenic MYC in the driver's seat. Signal Transduct. Targeted Ther. *5*, 124.
20. Dang, C.V. (2012). MYC on the path to cancer. Cell *149*, 22–35.
21. Chen, H., Liu, H., and Qing, G. (2018). Targeting oncogenic Myc as a strategy for cancer treatment. Signal Transduct. Targeted Ther. *3*, 5.

22. Li, Q., Pan, S., Xie, T., and Liu, H. (2021). MYC in T-cell acute lymphoblastic leukemia: functional implications and targeted strategies. Blood science *3*, 65–70.
23. Farrell, A.S., and Sears, R.C. (2014). MYC degradation. Cold Spring Harbor perspectives in medicine *4*.
24. Sears, R., Nuckolls, F., Haura, E., Taya, Y., Tamai, K., and Nevins, J.R. (2000). Multiple Ras-dependent phosphorylation pathways regulate Myc protein stability. Genes & development *14*, 2501–2514.
25. Jiang, J., Wang, J., Yue, M., Cai, X., Wang, T., Wu, C., Su, H., Wang, Y., Han, M., Zhang, Y., et al. (2020). Direct Phosphorylation and Stabilization of MYC by Aurora B Kinase Promote T-cell Leukemogenesis. Cancer Cell *37*, 200–215.e205.
26. Gregory, M.A., Qi, Y., and Hann, S.R. (2003). Phosphorylation by glycogen synthase kinase-3 controls c-myc proteolysis and subnuclear localization. J. Biol. Chem. *278*, 51606–51612.
27. Welcker, M., Orian, A., Jin, J., Grim, J.E., Harper, J.W., Eisenman, R.N., and Clurman, B.E. (2004). The Fbw7 tumor suppressor regulates glycogen synthase kinase 3 phosphorylation-dependent c-Myc protein degradation. Proceedings of the National Academy of Sciences of the United States of America *101*, 9085–9090.
28. Yada, M., Hatakeyama, S., Kamura, T., Nishiyama, M., Tsunematsu, R., Imaki, H., Ishida, N., Okumura, F., Nakayama, K., and Nakayama, K.I. (2004). Phosphorylation-dependent degradation of c-Myc is mediated by the F-box protein Fbw7. EMBO J. *23*, 2116–2125.
29. Akhoondi, S., Sun, D., von der Lehr, N., Apostolidou, S., Klotz, K., Maljukova, A., Cepeda, D., Fiegl, H., Dafou, D., Marth, C., et al. (2007). FBXW7/hCDC4 is a general tumor suppressor in human cancer. Cancer Res. *67*, 9006–9012.
30. Guo, H., Xu, J., Xing, P., Li, Q., Wang, D., Tang, C., Palhais, B., Roels, J., Liu, J., Pan, S., et al. (2023). RNA helicase DHX15 exemplifies a unique dependency in acute leukemia. Haematologica *108*, 2029–2043.
31. Toczydlowska-Socha, D., Zielinska, M.M., Kurkowska, M., Astha, Almeida, C.F., Stefaniak, F., Purta, E., and Bujnicki, J.M. (2018). Human RNA cap1 methyltransferase CMTr1 cooperates with RNA helicase DHX15 to modify RNAs with highly structured 5′ termini. Philosophical transactions of the Royal Society of London. Series B, Biological sciences *373*.
32. Inesta-Vaquera, F., Chaugule, V.K., Galloway, A., Chandler, L., Rojas-Fernandez, A., Weidlich, S., Peggie, M., and Cowling, V.H. (2018). DHX15 regulates CMTR1-dependent gene expression and cell proliferation. Life Sci. Alliance *1*, e201800092.
33. Niu, Z., Jin, W., Zhang, L., and Li, X. (2012). Tumor suppressor RBM5 directly interacts with the DExD/H-box protein DHX15 and stimulates its helicase activity. FEBS Lett. *586*, 977–983.
34. Liberzon, A., Birger, C., Thorvaldsdóttir, H., Ghandi, M., Mesirov, J.P., and Tamayo, P. (2015). The Molecular Signatures Database (MSigDB) hallmark gene set collection. Cell systems *1*, 417–425.
35. Combs, D.J., Nagel, R.J., Ares, M., Jr., and Stevens, S.W. (2006). Prp43p is a DEAH-box spliceosome disassembly factor essential for ribosome biogenesis. Mol. Cell Biol. *26*, 523–534.
36. Farrell, A.S., and Sears, R.C. (2014). MYC degradation. Cold Spring Harbor perspectives in medicine *4*, a014365.
37. Hondele, M., Sachdev, R., Heinrich, S., Wang, J., Vallotton, P., Fontoura, B.M.A., and Weis, K. (2019). DEAD-box ATPases are global regulators of phase-separated organelles. Nature *573*, 144–148.
38. Shen, C., Li, R., Negro, R., Cheng, J., Vora, S.M., Fu, T.M., Wang, A., He, K., Andreeva, L., Gao, P., et al. (2021). Phase separation drives RNA virus-induced activation of the NLRP6 inflammasome. Cell *184*, 5759–5774.e5720.
39. Dose, M., Khan, I., Guo, Z., Kovalovsky, D., Krueger, A., von Boehmer, H., Khazaie, K., and Gounari, F. (2006). c-Myc mediates pre-TCR-induced proliferation but not developmental progression. Blood *108*, 2669–2677.
40. Pereira, B., Billaud, M., and Almeida, R. (2017). RNA-Binding Proteins in Cancer: Old Players and New Actors. Trends in cancer *3*, 506–528.
41. Elcheva, I.A., and Spiegelman, V.S. (2021). Targeting RNA-binding proteins in acute and chronic leukemia. Leukemia *35*, 360–376.
42. Silverman, E., Edwalds-Gilbert, G., and Lin, R.J. (2003). DExD/H-box proteins and their partners: helping RNA helicases unwind. Gene *312*, 1–16.
43. Opatz, S., Bamopoulos, S.A., Metzeler, K.H., Herold, T., Ksienzyk, B., Bräundl, K., Tschuri, S., Vosberg, S., Konstandin, N.P., Wang, C., et al. (2020). The clinical mutatome of core binding factor leukemia. Leukemia *34*, 1553–1562.
44. Faber, Z.J., Chen, X., Gedman, A.L., Boggs, K., Cheng, J., Ma, J., Radtke, I., Chao, J.R., Walsh, M.P., Song, G., et al. (2016). The genomic landscape of core-binding factor acute myeloid leukemias. Nat. Genet. *48*, 1551–1556.
45. Jing, Y., Nguyen, M.M., Wang, D., Pascal, L.E., Guo, W., Xu, Y., Ai, J., Deng, F.M., Masoodi, K.Z., Yu, X., et al. (2018). DHX15 promotes prostate cancer progression by stimulating Siah2-mediated ubiquitination of androgen receptor. Oncogene *37*, 638–650.
46. Wang, Y., He, K., Sheng, B., Lei, X., Tao, W., Zhu, X., Wei, Z., Fu, R., Wang, A., Bai, S., et al. (2021). The RNA helicase Dhx15 mediates Wnt-induced antimicrobial protein expression in Paneth cells. Proceedings of the National Academy of Sciences of the United States of America *118*.
47. Tago, K., Funakoshi-Tago, M., Itoh, H., Furukawa, Y., Kikuchi, J., Kato, T., Suzuki, K., and Yanagisawa, K. (2015). Arf tumor suppressor disrupts the oncogenic positive feedback loop including c-Myc and DDX5. Oncogene *34*, 314–322.
48. Herranz, D., Ambesi-Impiombato, A., Palomero, T., Schnell, S.A., Belver, L., Wendorff, A.A., Xu, L., Castillo-Martin, M., Llobet-Navás, D., Cordon-Cardo, C., et al. (2014). A NOTCH1-driven MYC enhancer promotes T cell development, transformation and acute lymphoblastic leukemia. Nat. Med. *20*, 1130–1137.
49. Dutta, A., Zhao, B., and Love, P.E. (2021). New insights into TCR β-selection. Trends Immunol. *42*, 735–750.
50. Weng, A.P., Millholland, J.M., Yashiro-Ohtani, Y., Arcangeli, M.L., Lau, A., Wai, C., Del Bianco, C., Rodriguez, C.G., Sai, H., Tobias, J., et al. (2006). c-Myc is an important direct target of Notch1 in T-cell acute lymphoblastic leukemia/lymphoma. Genes & development *20*, 2096–2109.
51. Su, H., Hu, J., Huang, L., Yang, Y., Thenoz, M., Kuchmiy, A., Hu, Y., Li, P., Feng, H., Zhou, Y., et al. (2018). SHQ1 regulation of RNA splicing is required for T-lymphoblastic leukemia cell survival. Nat. Commun. *9*, 4281.
52. Subramanian, A., Tamayo, P., Mootha, V.K., Mukherjee, S., Ebert, B.L., Gillette, M.A., Paulovich, A., Pomeroy, S.L., Golub, T.R., Lander, E.S., and Mesirov, J.P. (2005). Gene set enrichment analysis: a knowledge-based approach for interpreting genome-wide expression profiles. Proc. Natl. Acad. Sci. USA *102*, 15545–15550.

STAR★METHODS

KEY RESOURCES TABLE

REAGENT or RESOURCE	SOURCE	IDENTIFIER
Antibodies		
Rabbit polyclonal anti-DHX15/prp43	Abcam	Cat# ab70454; RRID: AB_2261638
Mouse monoclonal anti-DHX15	Santa Cruz Biotechnology	Cat# sc-271686; RRID: AB_10707990
Rabbit polyclonal anti-c-Myc (N-262)	Santa Cruz Biotechnology	Cat# sc-764; RRID: AB_631276
Rabbit monoclonal anti-c-Myc	ABclonal	Cat# A19032; RRID: AB_2862524
Rabbit polyclonal anti-FBXW7	Abcam	Cat# ab109617; RRID: AB_2687519
Rabbit polyclonal anti-UBC	ABclonal	Cat# A3207; RRID: AB_2764989
Mouse monoclonal anti-FLAG-tag	Sigma-Aldrich	Cat# F1804; RRID: AB_262044
Mouse monoclonal anti-HA-tag	ABclonal	Cat# AE008; RRID: AB_2770404
Mouse monoclonal anti-Myc-tag	ABclonal	Cat# AE010; RRID: AB_2770408
HRP-conjugated monoclonal anti-HA-tag (3F10)	Roche	Cat# 12013819001; RRID: AB_390917
Rabbit monoclonal anti-β-Actin	ABclonal	Cat# AC026; RRID: AB_2768234
Bacterial and virus strains		
BL21 (DE3) Competent *E. coli*	Thermo Fisher Scientific	Cat# C601003
DH5α Competent *E. coli*	Thermo Fisher Scientific	Cat# 12297016
Chemicals, peptides, and recombinant proteins		
Cycloheximide	Sigma-Aldrich	Cat# C7698
MG132	Selleck	Cat# S2619
Recombinant His-tag DHX15	This paper	N/A
Recombinant GST-tag MYC	This paper	N/A
Critical commercial assays		
Annexin V-FITC Apoptosis Kit	BioVision	Cat# K201
iTaq Universal SYBR Green Supermix	Bio-Rad	Cat# 1725124
Lipofectamine 2000	Thermo Fisher Scientific	Cat# 11668027
ReverTra Ace qPCR RT kit	TOYOBO	Cat# FSQ-101
Deposited data		
Mass spectrometry analysis	This paper	PXD046692
Raw sequencing data	This paper	GSE247720
Raw sequencing data	Guo et al.[30]	GSE208746
Experimental models: Cell lines		
293T	ATCC	Cat# ACS-4500
CUTLL1	Weng et al.[50]	N/A

(*Continued on next page*)

Continued

REAGENT or RESOURCE	SOURCE	IDENTIFIER
KOPTK1	Weng et al.[50]	N/A
Kasumi-1	ATCC	Cat# CRL-2724
HL-60	ATCC	Cat# CCL-240
OCI-AML3	Cobioer (Nanjing, China)	Cat# CBP60817
RKO	ATCC	Cat# CRL-2577
H1299	ATCC	Cat# CRL-5803
Experimental models: Organisms/strains		
Mouse: NPG (NOD.Cg-Prkdc^{scid} Il2rg^{tm1Vst}/Vst)	Beijing Vitalstar Biotechnology	Cat# VS000187
Oligonucleotides		
See Table S1	This paper	N/A
Software and algorithms		
FlowJo	Tree Star	https://www.flowjo.com/
Gene Set Enrichment Analysis	Subramanian et al.[52]	http://software.broadinstitute.org/gsea/index.jsp
Graphpad Prism 8	Graphpad software	https://www.graphpad.com/
ImageJ	ImageJ: Image Processing and Analysis in Java	https://imagej.nih.gov/ij/

RESOURCE AVAILABILITY

Lead contact

Further information and requests for resources and reagents should be directed to and will be fulfilled by the lead contact, Hudan Liu (hudanliu@whu.edu.cn).

Materials availability

This study did not generate new unique reagents.

Data and code availability

Data: The raw data for the RNA-seq presented in this publication have been deposited in Gene Expression Omnibus (GEO: GSE247720). The mass spectrometry data have been deposited to the ProteomeXchange Consortium with the dataset identifier PXD046692.

Code: This paper does not report original code.

Any additional information required to reanalyze the data reported in this paper is available from the lead contact upon request.

EXPERIMENTAL MODEL AND STUDY PARTICIPANT DETAILS

Cell lines

Human T-ALL CUTLL1, KOPTK1 and AML Kasumi-1, HL-60, OCI-AML3 cell lines were grown in RPMI-1640 (Gibco) supplemented with 10% fetal bovine serum (FBS, Hyclone), 1% penicillin/streptomycin (Hyclone), 1% non-essential amino acids (Gibco), 2mM L-glutamine (Sigma), 1 mM sodium pyruvate (Sigma) and 55 μM β-mercaptoethanol (Sigma). RKO, H1299 and 293T cells were maintained in Dulbecco's modified Eagle's medium (DMEM, Gibco) containing 10% FBS (Hyclone) and 1% penicillin/streptomycin (Hyclone). All cell lines were authenticated using short tandem repeat (STR) analysis, cultured for fewer than 3 months after resuscitation, and tested for mycoplasma contamination once a month using PCR.

Animals

In the present study, immunocompromised NOD.Cg-Prkdc^{scid} Il2rg^{tm1Vst}/Vst (NPG) mice were used for T-cell reconstitution. Female mice (4-5 weeks old, 19±1.5g) were obtained from Beijing Vitalstar Biotechnology and were maintained in Specific Pathogen Free (SPF) animal facility of Medical Research Institute, Wuhan University. All mice were housed in groups of 3–4 in standard individually ventilated (IVC) cages in rooms with temperature maintained in 20-22°C and with 14h light and 10h dark cycles. All animal experiments were performed under animal ethical regulations and the study protocol was approved by the Institutional Animal Care and Use Committee of Wuhan University.

Microbe strains

E. coli DH5α or BL21 (DE3) competent cells were transformed and grown on plates of LB Agar with Ampicillin or Kanamycin 100 mg/mL for plasmid selection at 37°C.

METHOD DETAILS

Lentiviral and retroviral transduction

Lentiviral production and transduction were performed as described.[25,51] For viral production, lentiviral vectors (pLKO.1 for shRNA, pHAGE and pCDH for overexpression) were used for plasmid construction and transfected into 293T cells simultaneously with helper plasmids (pMD2.G and psPAX2). Retroviral vector MigR1 was used for plasmid construction and transfected into 293T cells together with packaging plasmids (pCgp and pHIT). Viral supernatants were generally collected 48 hr post transfection, and appropriate amount was added into two million cells suspended in 2 mL medium with the presence of 6 μg/mL polybrene (Sigma). After culture for 30 min, cells were then subjected to centrifugation at 1000 × g (rcf) for 90 min at 32°C.[30] Cell pellets were supplemented with 1 mL fresh medium and continued culture for at least 48 hr to achieve efficient gene silencing or overexpression.

RNA extraction and quantitative real-time PCR

Total cellular RNA was extracted using TRIzol (Thermo Fisher Scientific) and random primed RNAs (1 μg) were reverse transcribed with the ReverTra Ace qPCR RT Kit (TOYOBO) according to the manufacturer's instructions. Quantitative PCR was conducted using FAST SYBR Green Master Mix (Bio-Rad) on CFX Connect Real-Time PCR System (Bio-Rad). Relative expression of the mRNA was calculated by $2^{-\Delta\Delta Ct}$ method and normalized to *ACTB*. Specific PCR primer sequences were listed in Table S1.

Immunoblotting

Total cell lysates were prepared with RIPA lysis buffer containing protease inhibitors. 30-50 μg total cellular proteins were subjected to SDS-PAGE gel and transferred to polyvinylidene difluoride membrane (Bio-Rad). After being blocked with 5% fat free milk, blots were generally incubated with primary antibodies at 4°C overnight. Appropriate horseradish peroxidase conjugated secondary antibodies were applied for 1 hr at room temperature before detection with Clarity Western ECL Substrate (Bio-Rad). Densitometric analyses of protein abundance were determined by ImageJ software.

Co-immunoprecipitation

Cells were lysed with lysis buffer (50 mM Tri-HCl pH 7.4, 150 mM NaCl, 1 mM EDTA, 1% NP-40, 1 mM DTT and protease inhibitor cocktail) and placed on ice for 30 min before sonication on Scientz-650E. After centrifugation to remove debris, 1 mg of crude lysate was incubated with antibodies conjugated to Protein G beads (GE Healthcare) overnight at 4°C. Precipitated beads were then washed three times with lysis buffer and boiled in 2×SDS loading buffer before SDS-PAGE and immunoblot analysis. For denaturing IP to detect MYC protein polyubiquitylation, cells were lysed with 100 μL lysis buffer in the presence of 1% SDS and then denatured at 95°C for 5 min. A portion of cell lysates (20 μL) were saved for immunoblot analysis to detect the expression of MYC proteins. The rest of cell lysates (80 μL) were diluted with 1 mL lysis buffer and immunoprecipitated with specific antibodies conjugated to Protein G beads. Protein G beads associated proteins were analyzed by SDS-PAGE and immunoblotting.

Immunofluorescence

Cells were fixed on the cover clip with 4% paraformaldehyde for 15 min, and permeabilized with 0.2% Triton X-100 in PBS for 5 min. Fixed cells were then blocked with 3% BSA in PBS for 1 h, before incubation with anti-DHX15 or anti-MYC antibody at 4°C overnight. Cells were subsequently stained with Fluo-555 (1:200, Cell Signaling Technology) conjugated anti-rabbit secondary antibody or Fluo-488 (1:200, Cell Signaling Technology) conjugated anti-mouse secondary antibody for 1 h. After washing three times with PBS in dark, cells were mounted with DAPI Fluoromount-G (Yeasen). Immunofluorescence signals were detected by confocal microscopy (Nikon Eclipse, Japan).

Time-course analysis of MYC degradation

293T cells with *DHX15* depletion or overexpression were subjected to cycloheximide (CHX, Sigma) treatment (50 μg/mL) before harvest at specific time-points. Collected cells were immediately lysed in RIPA buffer containing protease inhibitor cocktail and centrifuged to remove debris as described.[25] Crude extract was subsequently used for immunoblotting. MYC protein band densities were quantified by ImageJ software and normalized to ACTIN.

In vivo T-cell reconstitution

The procedure for *in vivo* T-cell reconstitution was based on previous publications.[48] Bone marrow lineage negative (Lin^-) cells from $Dhx15^{fl/fl}$ or *Dhx15* KO (*Lck*-cre $Dhx15^{fl/fl}$) mice were enriched using Lineage Cell Depletion Kit (Miltenyi Biotec), and pre-stimulated for 24 hr in DMEM (Gibco) containing 20% FBS (Gibco), 1% penicillin/streptomycin (Hyclone), 20 ng/mL mFLT3-L, 20 ng/mL mTPO and 100 ng/mL mSCF (PeproTech). Cells were then transduced with MigR1-Myc or MigR1 retroviruses (details in "Lentiviral and retroviral transduction"), and transplanted into irradiated (1.5 Gray) female NOD.Cg-$Prkdc^{scid}$ $Il2rg^{tm1Vst}$/Vst (NPG) mice. T-cell lineage reconstitution was assessed 7 weeks after transplant in peripheral blood by flow cytometry.

RNA sequencing

Total RNA was extracted using TRIzol reagent (Thermo Fisher Scientific) and subjected to quality control for RNA integrity by Agilent Bioanalyzer 2100 system (Agilent Technologies). Total RNA was further purified by RNAClean XP Kit (Beckman Coulter) and RNase-Free DNase Set (QIAGEN). Poly(A)+ RNA libraries were constructed using VAHTS Universal V6 RNA-seq Library Prep Kit (Vazyme) and sequenced as 150 bp paired-end reads by Illumina NovaSeq 6000 (Annoroad Gene Technology Corporation). RNA-seq reads were analyzed by FastQC (version 0.11.9) and mapped to the human or mouse genome reference assembly (hg38 or mm10) using Hisat2 software (version 2.2.1). Differential gene expression was analyzed by DESeq2 (version 1.32.0).

Mass spectrometry analysis

Total cellular proteins extracted from CUTLL1 cells were subjected to immunoprecipitation using human DHX15 antibody (sc-271686, Santa Cruz). DHX15 and associated proteins were washed, and eluted with 0.2 M glycine pH 2.0. Eluted proteins were precipitated with acetone and digested with trypsin. The resulting peptides were desalted with the C18 Stage tips (Thermo Fisher Scientific), loaded onto an EASY-nanoLC system and analyzed in an Orbitrap Exploris 480 mass spectrometer equipped with the FAIMS Pro interface (Thermo Fisher Scientific). Mass spectrometry resolutions were set to 60,000 and mass range was set to 350-1500. Raw files were processed with Proteome Discoverer 2.4 (Thermo Fisher Scientific). Abundance of DHX15 associated proteins was quantified; $\log_2$FC and p value for individual protein were calculated via DEP package in R. The criteria of $\log_2$FC (DHX15 vs IgG) > 1 and p value < 0.05 was used to identify specific DHX15 interacting proteins. Top thirty DHX15 binding partners are shown in Table S2.

Flow cytometry analysis

For analysis of apoptotic cell death, cells were washed with PBS and resuspended in Annexin V binding buffer, and stained with Annexin V-FITC and propidium iodide (PI) at room temperature for 15 min. For immunophenotypic analysis, single-cell suspensions were prepared and stained with indicated antibodies at 4°C for 30 min. Fluorochrome-conjugated antibodies used were as follows: CD3ε (145-2C11, BioLegend), CD4 (RM4-5, BioLegend), CD8a (53-6.7, BD Pharmingen), CD25 (PC61, BD Horizon) and CD44 (IM7, BD Pharmingen). For intracellular staining of Myc, cells were first stained by specific surface antibodies and then fixed and permeabilized with BD Cytofix/Cytoperm Kit (BD Biosciences) according to the manufacturer's instructions. Cells were stained with a mouse anti-Myc antibody (9E10, Santa Cruz) and then an Alexa Fluor 647-conjugated anti-mouse IgG antibody (Cell Signaling Technology). Above all, acquisition was performed on an Accuri C6 (BD Biosciences) and flow cytometric sorting was conducted on a FACS Aria (BD Biosciences). Live cells were gated based on FSC and SSC characteristics. All acquired data were analyzed with FlowJo software (TreeStar).

QUANTIFICATION AND STATISTICAL ANALYSIS

All experiments were performed as at least three independent repeats and presented as mean ± SD. Data analysis were performed using Prism 8.0 software. Statistical significance was calculated by unpaired two-tailed Student's t-test between two groups or by one-way or two-way ANOVA with Tukey's corrections when comparing three or more groups. Statistical significance was set at $p < 0.05$. All of the statistical details of experiments can be found in the figure legends.